Published version:
doi.org/10.1016/j.clay.2013.05.006

Title: Fast aging treatment for the synthesis of hydrocalumites using microwaves.

List of authors and affiliations: Elena Pérez-Barrado[1,2,3], Maria Cinta Pujol[2], Magdalena Aguiló[2], Yolanda Cesteros[1], Francesc Díaz[2], Josep Pallarès[3], Lluís F. Marsal[3], Pilar Salagre*[1]

[1]Dept. Química Física i Inorgànica, EMAS, Universitat Rovira i Virgili (URV), Campus Sescelades, Marcel·lí Domingo, s/n, E-43007 Tarragona, Spain.

[2]Física i Cristal·lografia de Materials i Nanomaterials (FICMA-FICNA), EMAS, Universitat Rovira i Virgili (URV), Campus Sescelades, Marcel·lí Domingo, s/n, E-43007 Tarragona, Spain.

[3]Dept. d'Enginyeria Electrònica, Elèctrica i Automàtica, EMAS, Universitat Rovira i Virgili (URV), Campus Sescelades, Avda. Països Catalans, 26, E-43007 Tarragona, Spain.

(*) Corresponding author: Pilar Salagre. Tel: +34 977 559 571; fax: +34 977 559 563.

E-mail address: pilar.salagre@urv.cat.

Abstract:

Friedelt's salt $[Ca_2Al(OH)_6]Cl \cdot 2H_2O$, commonly known as hydrocalumite, was synthesized by co-precipitation following different aging treatments, using microwave irradiation or conventional heating and by refluxing or in autoclave, with the aim of decreasing the aging times (24 h) employed when aging by conventional heating or at room temperature. Hydrocalumites were characterized by XRPD, FT-IR, N_2 physisorption, ICP-OES, TEM, TEM-electron diffraction and TGA techniques. The use of microwaves favours a faster crystalline growth in the stacking direction whereas the use of autoclave improves the lamellar crystallinity. The highest crystallinity was found for the sample aged with microwave irradiation by autoclaving at 453 K for 1 h. This sample presented the highest crystallite size in the stacking direction (76 nm), the largest lamellar crystals (4000 nm) with *R*3*c* symmetry, and the highest dehydration- and dehydroxylation temperatures.

Keywords: Friedelt's salt, hydrocalumite, layered double hydroxide, microwaves, hydrothermal treatment, crystallinity.

1. Introduction

Layered double hydroxides (LDH) are anionic clays widely reported in literature. They are versatile materials with many applications in science: additives in polymers, catalysis, environmental treatments, medicine, etc (Del Hoyo, 2007; Guo et al., 2010). LDH have general formula $[M(II)_{1-x}M(III)_x(OH)_2]^{x+}(A^{n-}_{x/n})\cdot mH_2O$, where M(II) and M(III) are divalent and trivalent cations and A^{n-} the anion. The layers are positively charged due to trivalent cation substitution, which are compensated by the presence of anions in the interlamellar region, where water molecules are also located. In general, they form a mixture of oxides after calcination and have memory effect, which allows them to be reconstructed after calcination (Cavani et al., 1991). Hydrotalcites, with Mg and Al as divalent and trivalent cations, respectively, have been extensively studied, and used in many applications (Cavani et al., 1991; Figueras, 2004; Li and Duan, 2006; Tichit and Coq, 2003). However, in this study, we focus our attention into Friedelt's Salt, also called hydrocalumite (HC). Hydrocalumites have general formula $[Ca_2Al(OH)_6]Cl\cdot 2H_2O$, where the metals cations are usually calcium and aluminium (Rousellot et al., 2002). Typically, they play a significant role in cement and concrete industry in the composition of "AFm" phases, which contain hydrocalumite-like compounds expressed as hydrated calcium aluminates (Matschei et al., 2007; Raki et al., 2004; Raki et al., 2010). Interestingly, because of their basicity before and after calcination, they can be used as basic heterogeneous catalysts (Campos-Molina et al., 2010; Cota I. et al., 2010; Mora et al., 2010). Recently, it has been reported their use as absorbents for environmental purposes (Grover et al., 2010) and as inorganic framework for ceramic pigments (Domínguez et al., 2011).

Hydrocalumites can be synthesized with several types of anions in the interlamellar space, although chloride and nitrate anions are the most used (Frost et al., 2011; Vieille et al., 2003). In "AFm" phases, it is possible to find a wide range of anions: carbonate, sulphate, bromide, iodide and chromate (Mesbah et al., 2011). According to the structure, the interlamellar

distance and stability of the hydrocalumite can change depending on the anion. In view of the anion exchange capacity of LDH, HC with different anions can be used for different adsorbent applications (Zhou et al., 2012). The presence of carbonate ($–CO_3^{2-}$)- as interlamellar anion difficults greatly the anion exchange and delamination processes (Ma et al., 2006). An appropriate methodology for HC synthesis should always avoid the incorporation of carbonate in the interlamellar space and the calcite ($CaCO_3$) formation.

Recently, different approaches to synthesize HC have been reported. Sánchez-Cantú et al. prepared them from purchased hydrated lime and boehmite (Sánchez-Cantú et al., 2012). However, it was possible to identify boehmite and calcite phases in the final product; Kuwahara et al. recycled blast furnace slag as a precursor to obtain HC (Kuwahara et al., 2010) but they identified the presence of minor metals (Fe, Mn, Si and Ti) in the final chemical composition.

The most common synthetic procedure is the co-precipitation of Ca & Al salts at constant pH followed by an aging treatment at room temperature or by conventional heating; 353 K for 12 h (Radha et al., 2005), 333-338K for 24 h (Campos-Molina et al., 2010; Vieille et al., 2003), room temperature (RT) for 24 h (Grover et al., 2010) or RT for 48 h (Domínguez et al., 2011). Zhang et al. have optimized the modification of experimental variables such as pH, time, temperature and solvent for the production at a large-scale for the cement industry (Xu et al., 2011). They found the best results for samples aged at 343 K for 24 h that later were successfully scaled-up using SNAS (separate nucleation and aging steps) method at pH in the range of 10.5-11.5.

The use of microwaves irradiation in the aging process could be an excellent solution to decrease the long time of synthesis of hydrocalumites, since microwaves reduces enormously aging times but also provides much more crystallinity in the final material, as observed when applied to the synthesis of zeolitic materials and hydrotalcites (Ayala et al., 2011; Benito et al., 2006; Bergadà et al., 2007; Stoeger et al., 2012) or in the preparation of clays (hectorites and

saponites among others), where aging times have been remarkably decreased (Sánchez et al., 2012; Trujillano et al., 2010; Vicente et al., 2010).

The aim of this work was to synthesize Ca_2Al-Cl hydrocalumites by different aging treatments. In pursuit of finding a fast aging treatment that can lead to more crystalline hydrocalumites, we compare microwave irradiation versus conventional hydrothermal heating, and autoclave versus reflux conditions, at different times and temperatures.

2. Experimental

2.1 Synthesis of Ca_2Al-Cl hydrocalumites (HC)

Several hydrocalumites were synthesized by coprecipitation method at constant pH (Vieille et al., 2003) with a Ca/Al molar ratio of 2 and Cl^- as anion. In a typical synthesis, the samples were prepared with vigorous stirring, under N_2 atmosphere and using decarbonized water to prevent from $-CO_3^{2-}$ incorporation. A solution of 250 ml ethanol/water mixture (2:3 v/v) was placed into a 500 ml 4-neck round-bottom flask in an oil bath at 333 K. A 100 ml solution with the salts was prepared by mixing the appropriate amounts of 0.66 M $CaCl_2 \cdot 2H_2O$ (Sigma-Aldrich) and 0.33 M $AlCl_3 \cdot 6H_2O$ (Riedel-de Haën) solutions. Another solution of 2 M NaOH (Panreac) was used to keep pH constant at 11.5. The pH electrode and the two compensated pressure funnels for addition of the salts and the NaOH solution respectively, were connected to 3 of the necks of the round-bottom flask. N_2 was bubbled throw neck number 4 to avoid CO_2 incorporation. After complete addition of the salts, several aging procedures were performed using conventional or microwave heating and reflux or autoclave as recipients (Table 1). Samples were named starting with letters HC, corresponding to hydrocalumite, followed by letters R or A (refluxing or autoclave) for conventional heated samples and by RMW or MW (refluxing or autoclave) for microwaved samples. Finally, a number in subscript indicates the time of aging in hours whereas the number between parentheses is the temperature of aging. Additionally, another sample was synthesized at the

same preparation conditions than those employed for synthesizing sample $HCRMW_3(353)$ but without using inert atmosphere during the hydrothermal treatment ($HCRMW_3(353)B$). This sample was characterized by XRPD and FT-IR spectroscopy in order to detect the carbonate species bands. All samples were compared to $HCR_{24}(333)$, which was aged as reported in literature, by refluxing at 333 K for 24 h with conventional heating.

2.2 X-Ray powder diffraction (XRPD)

XRPD measurements were made using a Siemens D5000 diffractometer (Bragg–Brentano parafocusing geometry and vertical–goniometer) fitted with a curved graphite diffracted-beam monochromator and diffracted-beam Soller slits, a 0.06° receiving slit, and scintillation counter as a detector. The angular 2θ diffraction range was between 2º and 70º. Sample was dusted on to a low background Si(510) sample holder. The data were collected with an angular step of 0.05º at 3s per step and sample rotation. Cukα radiation was obtained from a copper X-ray tube operated at 40 kV and 30 mA.

2.3 Infrared spectroscopy (FTIR)

Infrared spectra were recorded on a Bruker-Equinox-55 FTIR spectrometer. Spectras were acquired by accumulating 32 scans at 4 cm^{-1} resolution in the range of 400–4000cm^{-1}. Samples were prepared by mixing the powdered solids with pressed KBr disks in a mass ratio of 1:250, and dried in an oven before measurements.

2.4 Inductively Coupled Plasma-Atomic Emission Spectroscopy (ICP-OES)

Ca/Al ratio has been analysed in an ICP-OES analyser (Induced Coupled Plasma – Optical Emission Spectroscopy) from Spectro Arcos. For the measurements, samples were introduced as a diluted solution into the analyser. The powders (50 mg) were solubilised with HNO_3 (2

ml), heated if necessary and brought to 25 ml volume. 1 ml of the solution was diluted into 25 ml. Standards were used to perform calibration curves. All analyses were made by triplicate.

2.5 N_2 physisorption

N_2-adsorption–desorption isotherms were recorded at 77 K using a Quantachrome Quadrasorb SI surface analyser. Prior to analysis samples were outgassed at 363 K. In a typical test, 0.2 g. of sample was used for analysis. Specific surface areas were calculated from BET (Brunauer-Emmett-Teller) method.Average pore size was calculated from BJH (Barrett-Joyner-Halenda) method. External surface area was calculated from t-plot (statistical Thickness) method.

2.6 Transmission electronic microscopy (TEM) and Electron diffraction

TEM images were collected using a JEOL 1011 Transmission Electron Microscope operating at 80 kV and magnification values of 12–60k. Samples were dispersed in ethanol, and a drop of resultant suspensions were poured on carbon coated-copper grids. Additionally, the same equipment was applied to make Selected Area Electron Diffraction (SAED). Camera length was 800 mm.

2.7 Thermogravimetric analysis (TG)

Thermogravimetric analyses were carried out in a Perkin Elmer TGA 7 microbalance equipped with a 273 – 1373 K programmable temperature furnace. The accuracy was ±1 μg. Each sample was heated in an N_2 flow (80 cm^3) from 298 K to 1000 K at 5 K/min.

3. Results and discussion

Figure 1 and 2 show the XRPD patterns of all samples. All reflexions belonged to the same crystalline phase, which was identified as hydrocalumite (HC) by comparison with the corresponding JCPDS file [035-0105]. This is a layered compound with formula

171 $[Ca_2Al(OH)_6]Cl{\cdot}2H_2O$, the structure of which is indexed in the trigonal lattice system and
172 belongs to group *R*3*c* (No 161) with theoretical *a* and *c* parameter values of 5.74 and 46.85 Å,
173 respectively. The layered structure is built by the periodical stacking of positively charged
174 $(Ca^{2+}, Al^{3+})(OH)_6$ octahedral layers and negatively charged interlayers with chloride and water
175 molecules (Rousselot et al., 2002). As observed in the diffraction patterns, the stacking
176 direction is along crystallographic *c* direction, since the samples present a strong preferential
177 orientation, showed by the high intensity of the (006) and (0012) peaks.
178 Additionally to the hydrocalumite phase, calcite was identified for sample $HCRMW_3(353)B$
179 by comparison with the calcite JCPDS file [083-0577], which showed a typical intense peak at
180 29.41º (Fig. 2b). The presence of calcite phase in this sample, that was prepared without N_2
181 atmosphere, confirmed that the use of inert atmosphere during synthesis was necessary to
182 obtain hydrocalumites as the only one crystalline phase.
183 The crystallite size along the stacking direction was calculated for (006) peak from the net
184 integral breadth of the reflections, β_i, according to the following formula that comes from the
185 Scherrer equation: $\beta_i=\lambda/\varepsilon\cos\theta$ where λ is the X-ray wavelength, ε is the crystallite size and θ
186 is the Bragg angle. This information is interesting in order to compare the growth rate for the
187 different aging processes used.
188 Table 2 shows the crystallite size along the stacking direction and the FWHM of (110)
189 reflection for all samples. The crystallite size was related to the crystal growth in the stacking
190 direction. In contrast, the crystallite size in the lamellar plane cannot be determined from
191 Scherrer equation using the FWHM of (110) reflection, because, as commented later in TEM
192 results, they are micrometric and the Scherrer equation is restricted to crystallites smaller than
193 500 nm (Cullity and Stock, 2001). However, the values of FWHM for (110) peak can be used
194 to compare the crystallinity of the samples (Table 2), since a decrease of FWHM values
195 involves an increase of crystallinity (Cullity and Stock, 2001).

196 Hydrocalumites aged using microwave irradiation by refluxing or in autoclave showed larger
197 crystallite sizes along the stacking direction than those aged by conventional heating under the
198 same conditions. The largest values (72-76 nm) corresponded to samples synthesized in
199 autoclave by microwaves ($HCMW_1(353)$, $HCMW_6(353)$ and $HCMW_1(453)$). Regarding
200 samples aged by refluxing, it was also possible to observe the positive effect of microwave
201 heating. Sample $HCRMW_3(353)$ showed higher crystallite size (50 nm) after 3 h of aging
202 compared to the conventional ones aged for 3 and 24 h (41 and 48 nm, respectively). Samples
203 aged in autoclave by conventional heating exhibited values of crystallite size in the stacking
204 direction (42 and 46 nm for samples $HCA_3(353)$ and $HCA_1(453)$, respectively) that were close
205 to the crystallite size of sample aged conventionally by refluxing for 24 h (48 nm) (Table 2).
206 This means that with autoclave under conventional heating (at 453 K for 1 h or at 353 K for 3
207 h), similar crystal growth can be obtained in less time. Therefore, microwave heating and
208 autoclave improve crystal growth in the stacking direction.
209 Comparing the values of FWHM corresponding to reflexion (110), the highest values (0.21-
210 0.20º) corresponded to samples aged by refluxing using conventional or microwave heating.
211 Therefore, the use of different heating method does not affect significatively the crystallinity of
212 the layer when refluxing was used. The range of FWHM values for samples prepared with
213 autoclave for conventional or microwave heating is 0.16-0.15º, which is slightly lower than that
214 obtained for the samples aged by refluxing (0.21-0.20º). Thus, higher crystallinity was observed
215 by using autoclave in comparison with refluxing. Among the samples aged by autoclave, higher
216 crystallinity was achieved with microwave irradiation. Therefore, samples aged using autoclave
217 together with microwave heating were the most crystalline.
218 In conclusion, autoclave and microwave irradiation enhances a faster production of more
219 crystalline lamellars at a lab-scale. Because of the faster synthesis, the absence of other phases
220 and the higher degree of crystallinity, the conditions of synthesis of $HCMW_1(453)$ were found
221 to be the most optima.

222 The lattice parameters of our synthesized samples *a* and *c* were calculated using literature
223 equations (Gay, 1972; Moore and Reynolds, 1989), from d_{110} and d_{006}, respectively (Table 2).
224 Lattice parameter *a* is related to the isomorphic substitution between Ca^{2+} and Al^{3+}, whereas *c*
225 parameter depends on the charge and size of the anion between the brucite layers (Cavani et
226 al., 1991). The fact that all values of *a* were practically the same for all hydrocalumites (Table
227 2) should be related to a similar stoichiometry for all samples. The same argument could be
228 applied to c values. In this case, with the same number and type of anion, the slight differences
229 observed in *c* values (Table 2) can be attributed to some differences in the hydration degree.
230 FT-IR spectra of all synthesised samples were very similar, showing the typical bands of these
231 kind of layered double hydroxides (Domínguez et al., 2011, Mora et al., 2011), summarized in
232 Table 3. Figure 3a shows the IR spectrum of sample $HCMW_1(453)$ as a representative sample.
233 According to the literature, it was possible to observe in the region 3000-3750 cm^{-1} a broad
234 band centered around 3500 cm^{-1} with peaks that are assigned to stretching vibrations of CaO-H
235 (3490 cm^{-1}) and AlO-H (3634 cm^{-1}). In the region between 500 and 800 cm^{-1} three intense
236 peaks, characteristic of metal bonds M-OH were also present. Additionally, in the region
237 between 1400 and 1650 cm^{-1} one characteristic band, centered at 1620 $cm^{-1}$was observed. This
238 band is assigned to deformation vibrations of water molecules. Finally, a small band around
239 1420 cm^{-1} was also observed in all spectra. This band could be related to some carbonation of
240 the sample, since this band corresponds to the C=O antisymmetrical stretching of the
241 carbonate species. Taking into account the low intensity of this band, probably carbonation
242 only takes place in the external surface of the particles during sample manipulation (Cota et
243 al., 2010), since calcite was not detected by X-Ray powder diffraction, as previously
244 commented.
245 In contrast, in figure 3b, IR spectrum of the sample $HCRMW_3(353)B$ showed the dramatic
246 effect of the absence of inert atmosphere during the synthesis and aging treatment of
247 hydrocalumites, since a significant increase of the intensity of the band at 1420 cm^{-1},

248 corresponding to carbonate species, was observed. Additionally, it was also possible to
249 identify other characteristics bands related to carbonates, at 710 cm^{-1} (bending angular) and at
250 875 cm^{-1} (bending non-planar). This agrees with the presence of calcite identified in this
251 sample by XRPD.
252 Table 4 shows the values corresponding to Ca/Al molar ratio measured by ICP. These values
253 are near to 2 for all samples. Therefore, with the different aging treatments it was possible to
254 obtain hydrocalumites with the expected stoichiometry, in agreement with the reagents ratio
255 used.
256 Adsorption/desorption isotherms were of type IV, according to IUPAC classification,
257 corresponding to mesoporous materials, for all synthesized hydrocalumites with hysteresis
258 loop type H3, associated to aggregates of plate-like particles leading to slid-shaped pores
259 (Cota et al., 2010). BET surface area, microporous area, determined by t-plot method, and
260 average pore radius values are given in Table 4. All samples presented low BET area and
261 depreciable measured values of microporosity, mainly due to the fact that the internal area in
262 the interlayer space cannot be measured due to the restriction for N_2 adsorption in this space.
263 However, BET area values can be related to the crystallinity of the samples. Thus, lower BET
264 area values (2 and 5 m^2/g) were obtained for the more crystalline samples, which were those
265 prepared with microwave irradiation in autoclave. Average pore radius values, determined by
266 BJH method, were between a maximum of 18.3 nm for $HCR_{24}(333)$ and a minimum of 10.1
267 nm for $HCMW_1(453)$. This lower value agrees with its higher crystallinity. However, for the
268 rest of samples, we did not observe a direct correlation between the average pore radium and
269 crystallinity (Campos-Molina et al., 2010; Domínguez et al., 2011).
270 TEM micrographs of all synthesized hydrocalumites (Figures 4 and 5) showed lamellar
271 structures with aggregated large particles as observed by the dark colour of the sheets. Sample
272 $HCR_{24}(333)$ (Fig. 4a), which was aged with conventional heating under 24 h of refluxing,
273 presented less defined hexagonal shape and very heterogeneous lamellar size distribution. This

274 can be related to its lower crystallinity that is a consequence of the aging conditions. In
275 contrast, sample HCA_3(353) (Fig 4b.), which was aged by conventional heating in autoclave,
276 exhibited a best definition of the hexagonal shape with more homogeneous lamellar sizes and
277 width values between 350 and 800 nm. Samples that were fast aged under microwave
278 irradiation $HCMW_1$(353) (Fig. 4c) and $HCMW_1$(453) (Fig. 4d) showed very well defined
279 hexagonal lamellars with larger sizes and width values around 1.6 μm for $HCMW_1$(353) and 4
280 μm for $HCMW_1$(453). In fact, this sample presented the lowest value of FWHM for the peak
281 (110) and the lowest BET surface area. Figure 5 shows electron diffraction pattern with the
282 presence of six equivalent reflections corresponding to (110) and equivalents (Fig. 5c) for
283 sample $HCMW_1$(453) (Fig. 5a). The electron diffraction pattern indicates a highly crystalline
284 sample, in agreement with the XRPD results and according to the defined hexagonal
285 morphology for hydrocalumites. Using the Shape utility that applies the Wulff theorem *R(hkl)*,
286 it has been modelized the crystal habit and indexed the faces (Fig. 5b). In conclusion, the
287 morphology, the crystallinity and the size of particles depended on the aged conditions used.
288 Figure 6 shows a representative thermogram of the synthesised hydrocalumites, which was
289 recorded from 353 to 1000 K after an isotherm of 30 min to exclude humidity adsorbed in the
290 surface of the samples. We can observe 3 of the 4 expected steps (Domínguez et al., 2011): i)
291 dehydration of interlamellar water, ii) dehydroxylation of the layers, iii) and iv) anion
292 decomposition. Due to the instrument safety limitations it was not possible to rise temperature
293 to see completion of the anion decomposition. For all hydrocalumites, the first and second
294 steps were well defined in the TGA curves and the values of mass loss were those expected for
295 the proposed stoichiometry: dehydration (12.8 %) and partial dehydroxylation (16 %),
296 according to the decomposition steps proposed in the literature (Domínguez et al., 2011).
297 The % of the second step was lower than that corresponding to the total dehydroxylation
298 (19.2 %). This was related to the formation of CaOHCl together with CaO and Al_2O_3 in the
299 2:2:1 ratio (Domínguez et al., 2011). Respect to anion decomposition, the mass loss value

obtained was lower than 13 %, since higher temperatures than 1000 K are necessary for total anion decomposition. Figure 7 depicts the temperatures of the maximum mass loss rates corresponding to the first and second TGA steps for all samples. The values of the temperature for the dehydration step were in the range 436- 457 K. The highest values were obtained for the most crystalline samples ($HCMW_1(453)$, $HCMW_6(353)$ and $HCMW_1(353)$). A higher order in the stacking direction can suppose stronger interactions for the interlamellar water, and consequently, higher temperatures should be necessary to remove it. With respect to the second mass loss, which corresponds to dehydroxylation, the temperature of the maximum mass loss rate was similar for all samples (601-613 K). However, again, the highest values were observed for the samples prepared using microwaves in autoclave. These samples presented larger lamellar size, as observed by TEM and higher crystallinity of the lamellas in agreement with the XPRD results

4. Conclusions

In this work, several hydrocalumites were synthesized by changing two variables, microwave or conventional heating and autoclave or refluxing. With the aim of synthetize faster a more crystalline material for future applications, we found that the sample $HCMW_1(453)$ prepared with microwaves by autoclave at 453 K for 1 h not only decreased significantly times of preparation compared to the conventional hydrocalumites reported in literature (aged at reflux for 24 h), but also presented high cristallinity, as observed by XRPD and TEM-electron diffraction. This agrees with its low surface BET area (2 m^2/g), its large defined hexagonal particles (4000 nm) and its highest temperature of dehydration and dehydroxylation observed by thermogravimetric analysis. In general, we can conclude that the use of microwaves for hydrocalumite synthesis favours a faster crystalline growth in the stacking direction whereas the use of autoclave improves the lamellar crystallinity (microwaves or conventional). Samples whose aging treatment was performed with microwave irradiation and in autoclave

326 ($HCMW_1$(453), $HCMW_6$(353) and $HCMW_1$(353)) exhibited the lowest values of BET surface
327 area (2, 5 and 5 m^2/g respectively) and the highest crystallinity. This characteristic was defined
328 by their crystallite size for (006) reflection since these samples presented the highest values
329 (762, 724 and 757 Å respectively), by their lowest FWHM for (110) reflection (0.15, 0.15 and
330 0.16º respectively) and by their well-defined hexagonal lamellas with the highest size
331 observed by TEM (>1600 nm).
332
333 **Acknowledgements**
334 The authors are grateful for the financial support of Ministerio de Economía y Competitividad,
335 FEDER Funds (CTQ2009-12520-C03-02, CTQ-2011-24610, TEC2012-34397,
336 CONSOLIDER HOPE project CSD2007-00007**,** TEC2010-21574-C02-02 and MAT2011-
337 29255-C02-02), the Catalan Government under project 2009SGR235 and Universitat Rovira i
338 Virgili scholarship program for PhD grant.
339
340
341
342
343
344
345
346
347
348
349
350
351

352 **References**

353 Ayala, A., Fetter, G., Palomares, E., Bosch, P., 2011. CuNi/Al hydrotalcites synthesized in
354 presence of microwave irradiation. Materials Letters 65 (11), 1663-1665.
355 Benito, P., Labajos, F.M., Rocha, J., Rives, V., 2006. Influence of microwave radiation on the
356 textural properties of layered doublé hydroxides. Microporous and Mesoporous Materials 94
357 (1-3), 148-158.
358 Bergadà, O., Vicente, I., Salagre, P., Cesteros, Y., Medina, F., Sueiras, J.E., 2007. Microwave
359 effect during aging on the porosity and basic properties of hydrotalcites. Microporous and
360 Mesoporous Materials 101 (3), 363-373.
361 Campos-Molina, M.J., Santamaría-González, J., Mérida-Robles, J., Moreno-Tost, R.,
362 Albuquerque, M.C.G., Bruque-Gámez, S., Rodríguez-Castellón, E., Jiménez-López, A.,
363 Maireles-Torres, P., 2010. Base Catalysts Derived from Hydrocalumite for the
364 Transesterification of Sunflower Oil. Energy Fuels 24 (2), 979–984.
365 Cavani, F., Trifirò F., Vaccari A., 1991. Hydrotalcite-type anionic clays: Preparation,
366 properties and applications. Catalysis Today 11 (2) 173-301.
367 Cota, I., Ramírez, E., Medina, F., Sueiras, J.E., Layrac, G., Tichit, D., 2010. New synthesis
368 route of hydrocalumite-type materials and their application as basic catalysts for aldol
369 condensation. Applied Clay Science 50 (4), 498-502.
370 Cullity, B.D., Stock, S.R., 2001. Elements of X-Ray Diffraction, third ed. Prentice Hall, New
371 Jersey.
372 Del Hoyo, C., 2007. Layered double hydroxides and human health: An overview. Applied
373 Clay Science 36 (1-3), 103–121.
374 Domínguez, M., Pérez-Bernal, M.E., Ruano-Casero, J.R., Barriga, C., Rives, V., Ferreira,
375 R.A.S., Carlos, L.D., Rocha J., 2011. Multiwavelength Luminescence in Lanthanide-Doped
376 Hydrocalumite and Mayenite. Chemistry of Materials 23 (7), 1993-2004.

377 Figueras, F., 2004. Base catalysis in the synthesis of fine chemicals. Topics in Catalysis 29,
378 (3–4), 189-196.
379 Frost, R. L., Palmer, S. J., Theiss, F., 2011. Synthesis and Raman spectroscopic
380 characterisation of hydrotalcites based on the formula $Ca_6Al_2(CO_3)(OH)_{16}\cdot 4H_2O$. Journal of
381 Raman Spectroscopy 42 (5), 1163-1167.
382 Gay, P., 1972. The Crystalline State, an Introduction, first ed. Oliver & Boyd, Edinburgh.
383 Guo, X., Zhang, F., Evans, D.G., Duan, X., 2010. Layered double hydroxide films: synthesis,
384 properties and applications. Chemical Communications 46 (29), 5197-5210.
385 Grover, K., Komarneni, S., Katsuki, H., 2010. Synthetic hydrotalcite-type and hydrocalumite-
386 type layered double hydroxides for arsenate uptake. Applied Clay Science 48 (4), 631-637.
387 Kuwahara, Y., Ohmichi, T., Kamegawa, T., Mori K., Yamashita, H., 2010. A novel
388 conversion process for waste slag: synthesis of a hydrotalcite-like compound and zeolite from
389 blast furnace slag and evaluation of adsorption capacities. Materials Chemistry 20 (24), 5052–
390 5062.
391 Li, F., Duan, X., 2006. Applications of Layered Double Hydroxides. Layered Double
392 Hydroxides. Structure and Bonding 119, 193–223.
393 Ma, R., Liu, Z., Li, L., Iyi, N., Sasaki, T., 2006. Exfoliating layered double hydroxides in
394 formamide: a method to obtain positively charged nanosheets. Journal of Materials Chemistry
395 16 (39), 3809-3813.
396 Matschei, T., Lothenbach, B., Glasser, F.P., 2007. The AFm phase in Portland cement.
397 Cement and Concrete Research 37 (2), 118-130.
398 Mesbah, A., Cau-dit-Coumes, C., Frizon, F., Leroux, F., Ravaux, J., Renaudin, G., 2011. A
399 New Investigation of the Cl^{-}–CO_3^{2-} Substitution in AFm Phases. Journal of the American
400 Ceramic Society 94 (6), 1901-1910.
401 Mora, M., López, M.I., Jiménez-Sanchidrián, C., Ruiz, J.R., 2010. Ca/Al Mixed Oxides as
402 Catalysts for the Meerwein–Ponndorf–Verley Reaction. Catalysis Letters 136 (3-4), 192-198.

403 Mora, M., López, M.I., Jiménez-Sanchidrián, C., Ruiz, J.R., 2011. Near- and mid-infrared
404 spectroscopy study of synthetic hydrocalumites. Solid State Sciences 13 (1), 101-105.
405 Moore, D.M., Reynolds, R.C., 1989. X-Ray Diffraction and the Identification and Analysis of
406 Clay Minerals, first ed. Oxford University Press, Oxford.
407 Radha, A.V., Kamath, P.V., Shivakumara, C., 2005. Mechanism of the anion exchange
408 reactions of the layered double hydroxides (LDHs) of Ca and Mg with Al. Solid State
409 Sciences 7 (10), 1180-1187.
410 Raki, L., Beaudoin, J., Alizadeh, R., Makar J., Sato, T., 2010. Cement and Concrete
411 Nanoscience and Nanotechnology. Materials 3 (2), 918-942.
412 Raki, L., Beaudoin, J.J., Mitchell, L., 2004. Layered double hydroxide-like materials:
413 nanocomposites for use in concrete. Cement and Concrete Research 34 (9), 1717-1724.
414 Rousselot, I., Taviot-Guého, C., Leroux, F., Léone, P., Palvadeau, P., Besse, J.P ., 2002.
415 Insights on the Structural Chemistry of Hydrocalumite and Hydrotalcite-like Materials:
416 Investigation of the Series $Ca_2M^{3+}(OH)_6Cl\cdot 2H_2O$ (M^{3+}: Al^{3+}, Ga^{3+}, Fe^{3+}, and Sc^{3+}) by X-Ray
417 Powder Diffraction. Journal of Solid State Chemistry 167 (1), 137-144.
418 Sánchez, T., Salagre, P., Cesteros, Y., Bueno-López, A., 2012. Use of delaminated hectorites
419 as supports of copper catalysts for the hydrogenolysis of glycerol to 1,2-propanediol.
420 Chemical Engineering Journal 179, 302–311.
421 Sánchez-Cantú, M., Pérez-Díaz, L. M., Tepale-Ochoa, N., González-Coronel, V. J., Ramos-
422 Cassellis, M. E., Machorro-Aguirre, D., Valente. J.S., 2012. Green synthesis of
423 hydrocalumite-type compounds and their evaluation in the transesterification of castor bean oil
424 and methanol. Fuel http://dx.doi.org/10.1016/j.fuel.2012.06.078
425 Stoeger, J. A., Palomino, M., Agrawal, K. V., Zhang, X., Karanikolos, G. N., Valencia, S.,
426 Corma, A., Tsapatsis, M., 2012. Oriented CoSAPO-5 Membranes by Microwave-Enhanced
427 Growth on TiO_2-Coated Porous Alumina. Angewandte Chemie International Edition 51 (10),
428 2470–2473.

Tichit, D., Coq, B., 2003. Catalysis by hydrotalcites and related materials. CATTECH 7 (6), 206-217.

Trujillano, R., Rico, E., Vicente, M.A., Herrero, M., Rives, V., 2010. Microwave radiation and mechanical grinding as new ways for preparation of saponite-like materials. Applied Clay Science 48 (1-2), 32-38.

Vicente, I., Salagre, P., Cesteros, Y., Sueiras, J.E., 2010. Microwave-assisted synthesis of saponite. Applied Clay Science 48 (1-2), 26–31.

Vieille, L., Rousselot, I., Leroux, F., Besse, J.P., Taviot-Guého, C., 2003. Hydrocalumite and Its Polymer Derivatives. 1. Reversible Thermal Behavior of Friedel's Salt: A Direct Observation by Means of High-Temperature in Situ Powder X-ray Diffraction. Chemistry of Materials 15 (23), 4361-4368.

Xu, S., Zhang, B., Chen, Z., Yu, J., Evans, D.G., Zhang, F., 2011. A General and Scalable Formulation of Pure CaAl-Layered Double Hydroxide via an Organic/Water Solution Route. Industrial & Engineering Chemistry Research 50 (11), 6567-6572.

Zhou, J.Z., Feng, L., Zhao, J., Liu, J., Liu, Q., Zhang, J., Qian, G., 2012. Efficient and controllable phosphate removal on hydrocalumite by multi-step treatment based on pH-dependent precipitation. Chemical Engineering Journal 185-186, 219-225.

Table 1. Aging treatments for hydrocalumites synthesis.

Nomenclature	Heating	Recipient	Temperature (K)	Time (h)
	Conventional/ Microwaves	Reflux/ Autoclave		
$HCR_{24}(333)$	Conventional	Reflux	333	24
$HCR_{3}(353)$	Conventional	Reflux	353	3
$HCRMW_{3}(353)$	Microwaves	Reflux	353	3
$HCA_{3}(353)$	Conventional	Autoclave	353	3
$HCA_{1}(453)$	Conventional	Autoclave	453	1
$HCMW_{1}(353)$	Microwaves	Autoclave	353	1
$HCMW_{6}(353)$	Microwaves	Autoclave	353	6
$HCMW_{1}(453)$	Microwaves	Autoclave	453	1

Table 2. Unit cell parameters and crystallographic characterization data obtained from XRPD of the HC synthesized in the present work.

Sample	**Crystallite Size (006) (nm)**	**FWHM (º) (110)**	**a (Å)**	**c (Å)**
HCR_{24}(333)	48	0.21	5.75	47.38
HCR_{3}(353)	41	0.20	5.74	47.35
$HCRMW_{3}$(353)	50	0.20	5.75	47.05
HCA_{3}(353)	42	0.16	5.74	47.17
HCA_{1}(453)	46	0.16	5.75	47.15
$HCMW_{1}$(353)	72	0.16	5.74	47.00
$HCMW_{6}$(353)	76	0.15	5.74	46.92
$HCMW_{1}$(453)	76	0.15	5.74	46.99

Table 3. IR band assignations of the HC synthesized in the present work.

Band identification	ν (cm^{-1})
OH stretching (AlO-H)	3638
OH stretching (CaO-H)	3493
deformation mode of water molecules	1622
C=O stretching	1414
metal-OH bonds	782
metal-OH bonds	584
metal-OH bonds	530

Table 4. ICP and Physisorption results of the HC synthesized in the present work.

Sample	**Ca/Al molar ratio**	**BET area (m^2/g)**	**Microporous area (m^2/g)**	**Average pore radius (nm)**
HCR_{24}(333)	1.99	9	1.52	18.3
HCR_3(353)	1.94	18	0.37	15.2
$HCRMW_3$(353)	2.00	7	0.21	14.8
HCA_3(353)	2.00	15	0.19	14.5
HCA_1(453)	1.95	12	0.32	11.9
$HCMW_1$(353)	1.88	5	0.26	13.0
$HCMW_6$(353)	1.87	5	0.42	16.9
$HCMW_1$(453)	1.84	2	0	10.1

Legends and captions:

- **Figure 1.** XRPD of the samples synthesized by conventional heating a) $HCR_{24}(333)$, b) $HCR_3(353)$, c) $HCA_1(453)$ d) $HCA_3(353)$. Hydrocalumite pattern: [JPDCS file: 035-0105].

- **Figure 2.** XRPD of the samples synthesized by microwaves irradiation a) $HCRMW_3(353)$, b) $HCRMW_3(353)B$, c) $HCMW_6(353)$, d) $HCMW_1(353)$, e) $HCMW_1(453)$. Hydrocalumite pattern: [JPDCS file: 035-0105], *: calcite characteristic peak at 29.41º.

-**Figure 3.** FTIR spectra of samples a) $HCRMW_3(353)$ aged without inert atmosphere, b) $HCMW_1(453)$ aged with inert atmosphere.

- **Figure 4.** TEM micrographs of samples a) $HCR_{24}(333)$, b) $HCA_3(353)$, c) $HCMW_1(353)$ and d) $HCMW_1(453)$.

- **Figure 5.** a) TEM micrograph of sample $HCMW_1(453)$, b) morphology of hydrocalumite, c) electron diffraction pattern.

- **Figure 6.** Thermal decomposition of hydrocalumite $HCMW_1(453)$. a) mass loss, b).first derivative of mass loss.

- **Figure 7.** Temperatures of the maximum mass loss rate for the derivative of first and second steps in the thermal decomposition of synthesized samples. In black filled circles, temperature of dehydratation step . In white filled rhombus, temperature of partial dehydroxylation step.

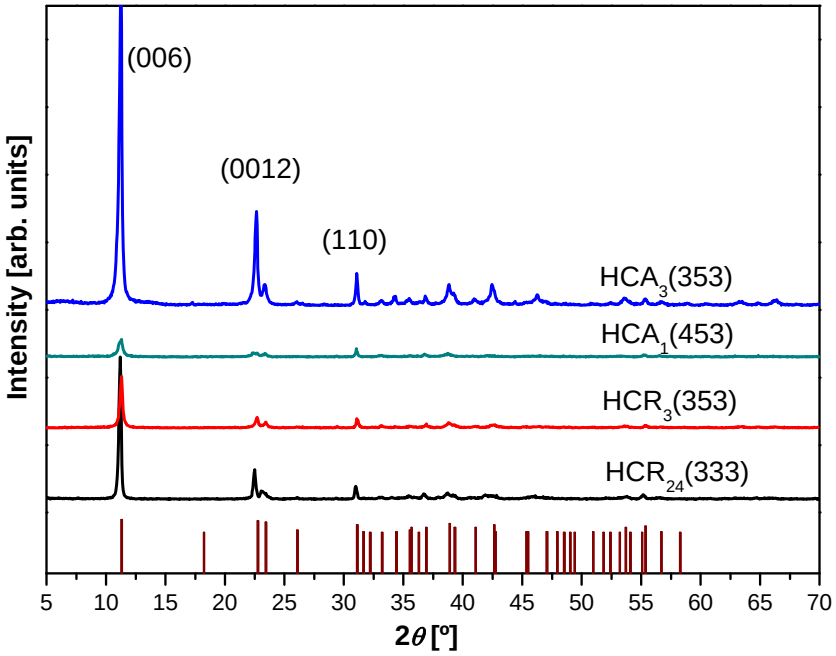
(006)
(0012)
(110)
HCA3(353)
HCA1(453)
HCR3(353)
HCR24(333)
Intensity [arb. units]
5
10
15
20
25
30
35
40
45
50
55
60
65
70
2θ [°]

Figure 1.

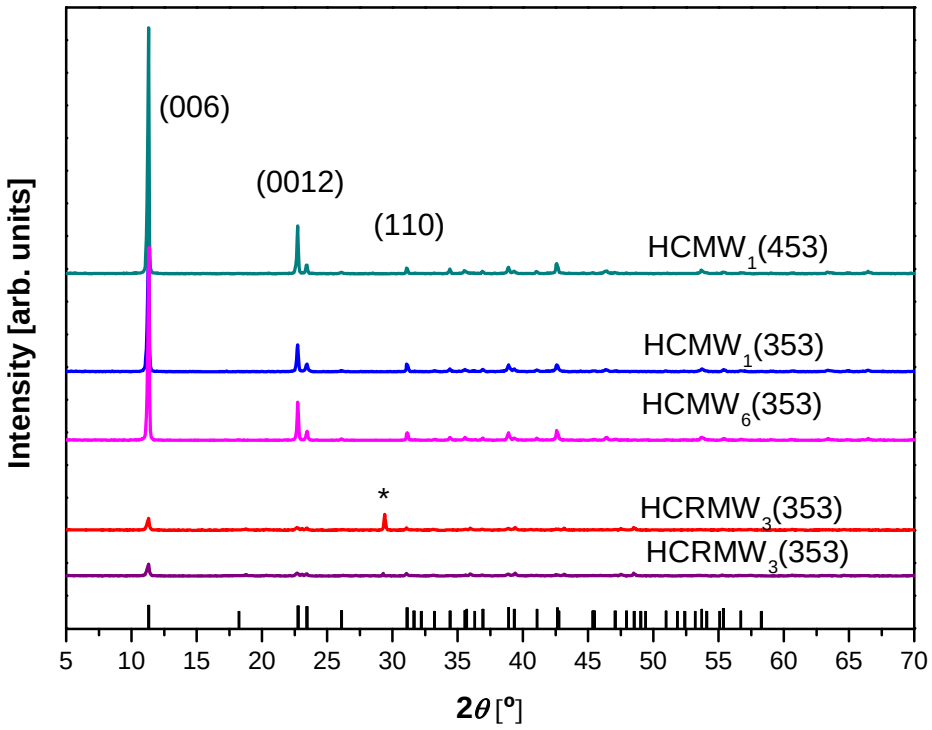
(006)
(0012)
(110)
HCMW1(453)
HCMW1(353)
HCMW6(353)
*
HCRMW3(353)
HCRMW3(353)
Intensity [arb. units]
5
10
15
20
25
30
35
40
45
50
55
60
65
70
2θ [º]

Figure 2.

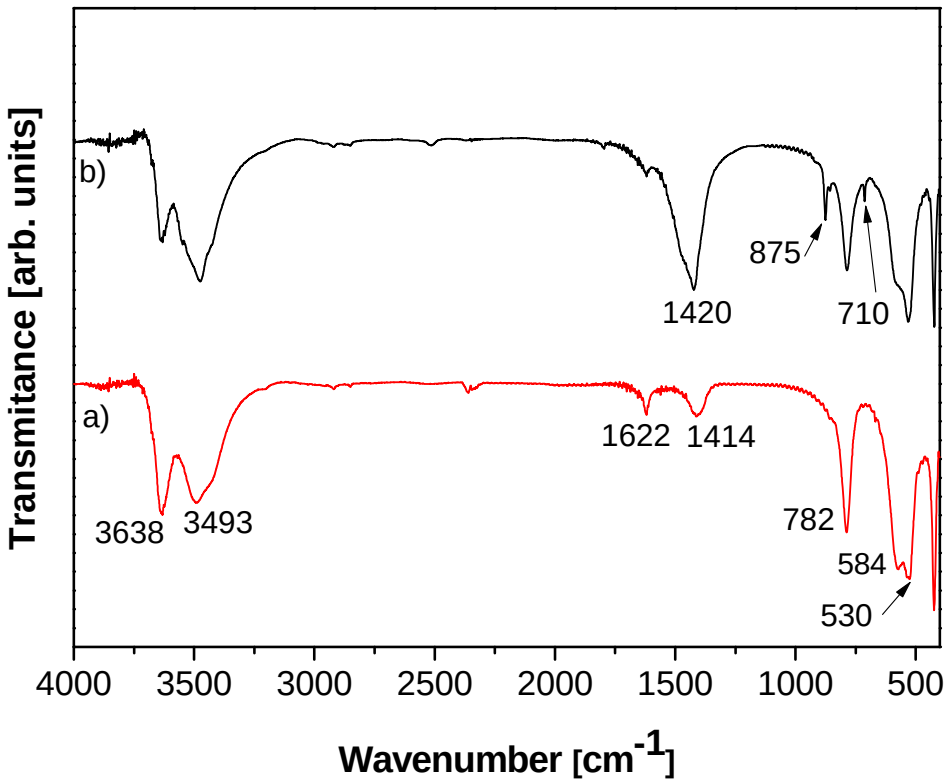
Transmitance [arb. units]
b)
a)
875
1420
710
1622
1414
3638
3493
782
584
530
4000
3500
3000
2500
2000
1500
1000
500
Wavenumber [cm-1]

Figure 3.

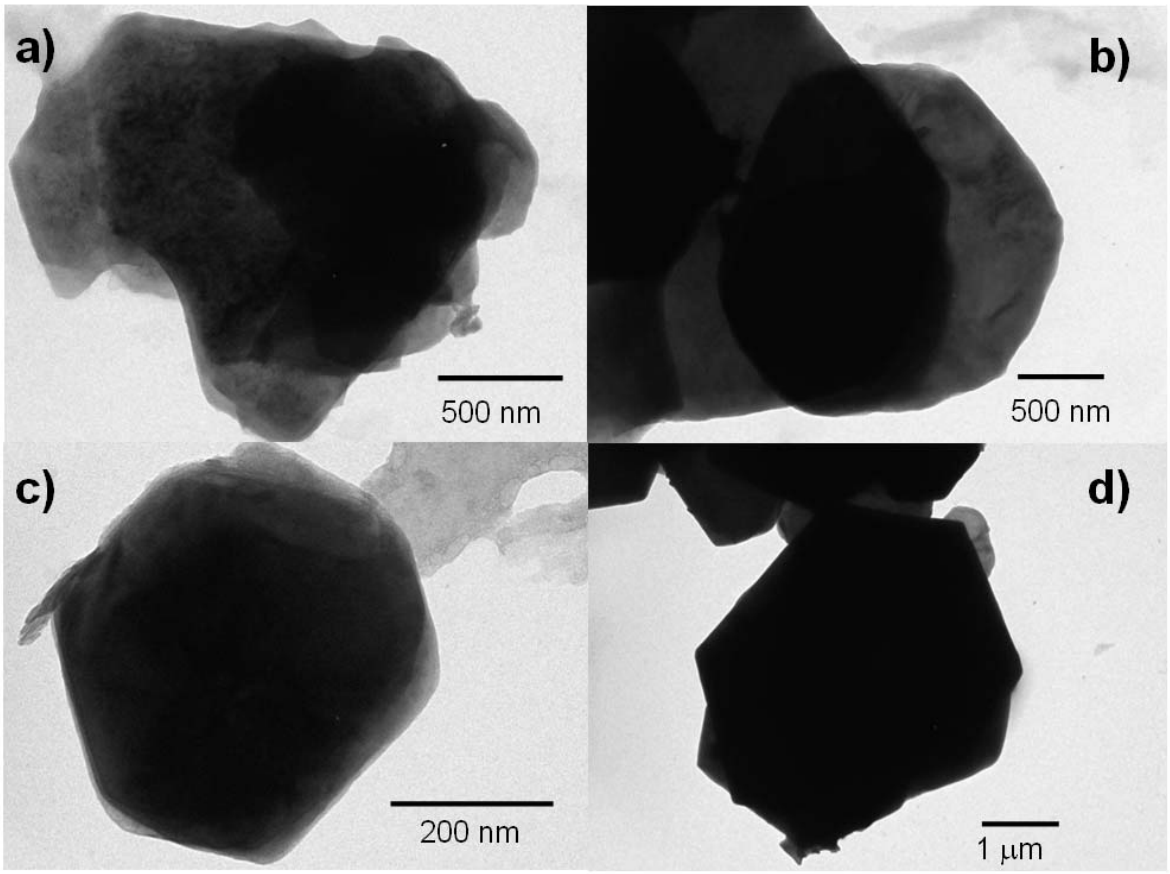

Figure 4.

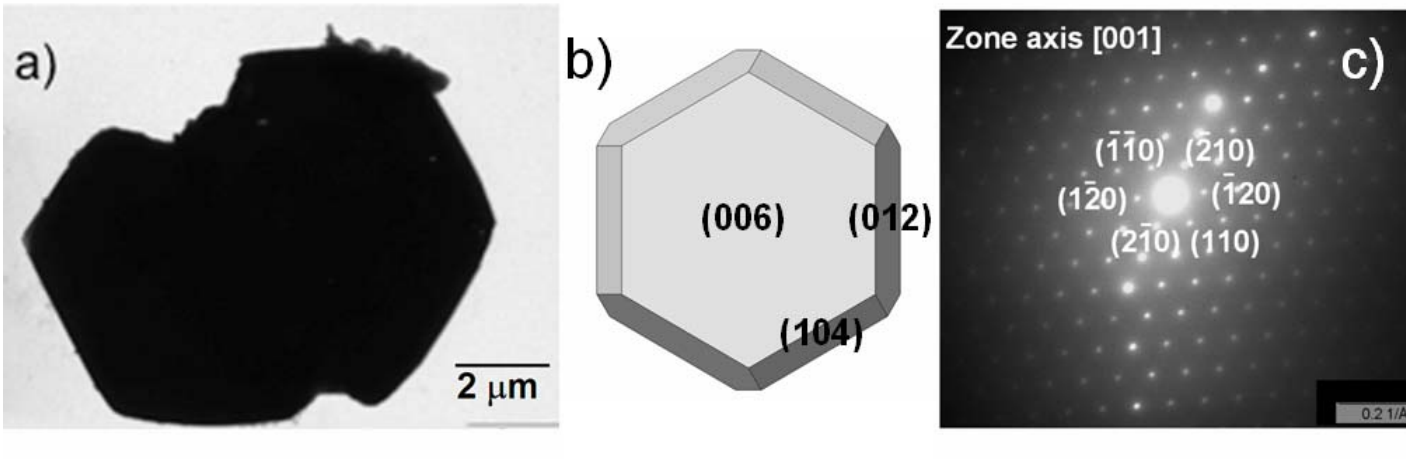

Figure 5.

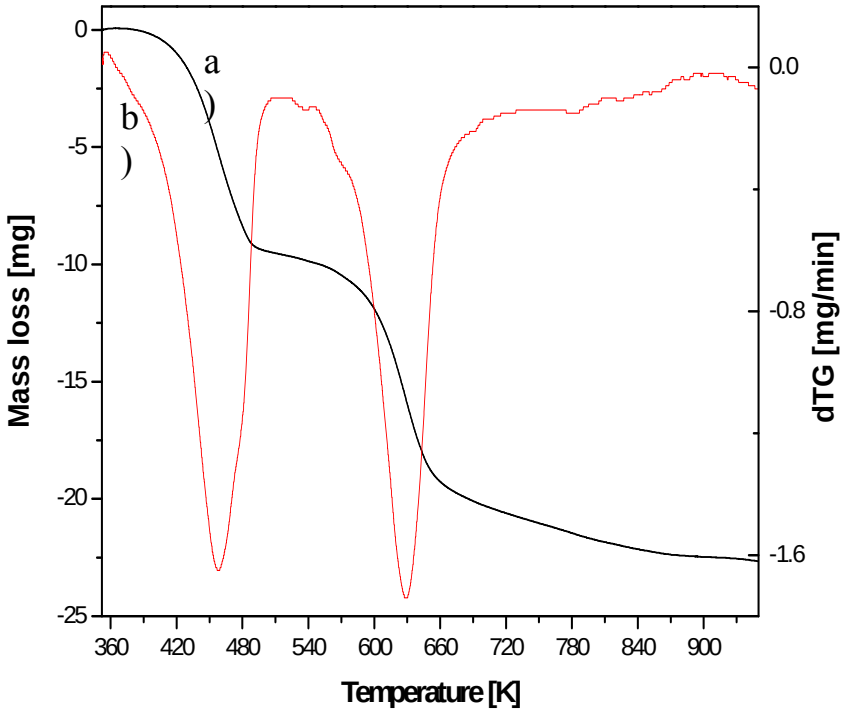
0
-5
-10
-15
-20
-25
Mass loss [mg]
a
)
b
)
0.0
-0.8
-1.6
dTG [mg/min]
360
420
480
540
600
660
720
780
840
900
Temperature [K]

Figure 6.

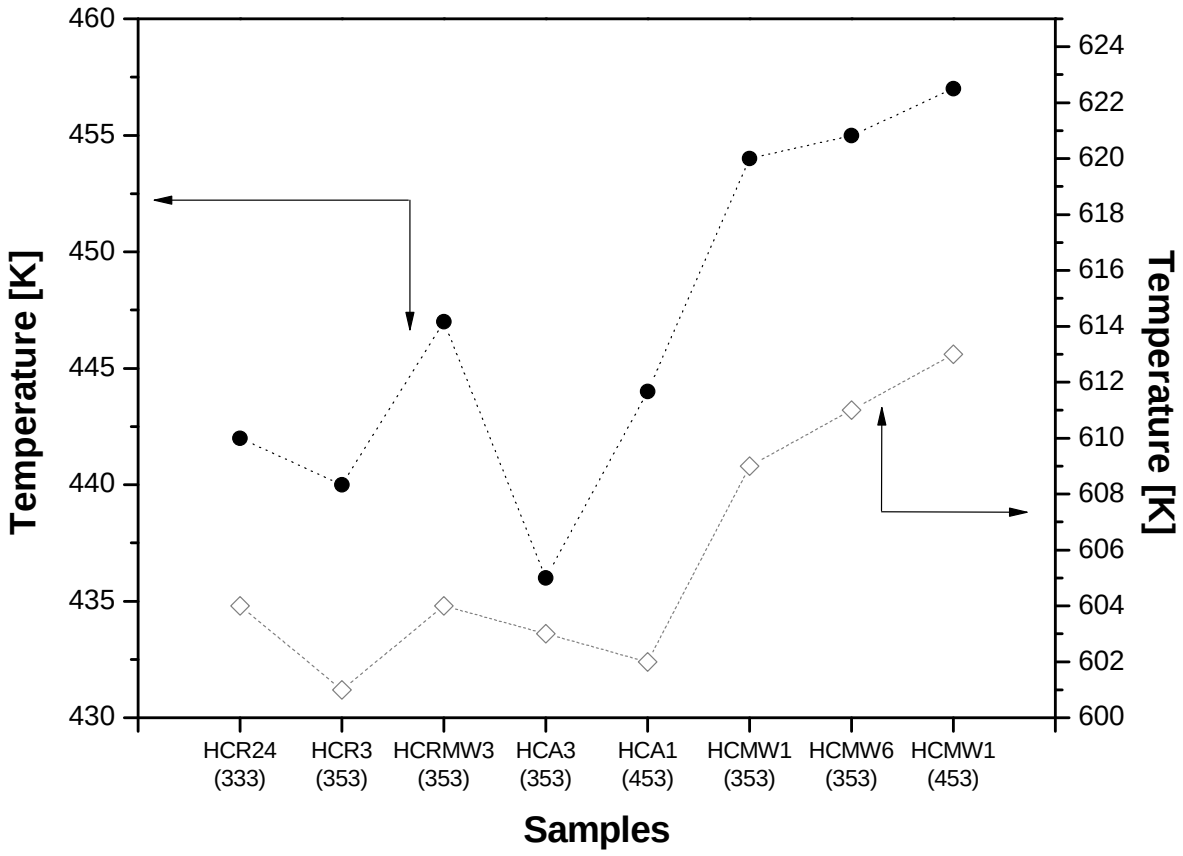
460
455
450
445
440
435
430
624
622
620
618
616
614
612
610
608
606
604
602
600
Temperature [K]
Temperature [K]
HCR24 (333)
HCR3 (353)
HCRMW3 (353)
HCA3 (353)
HCA1 (453)
HCMW1 (353)
HCMW6 (353)
HCMW1 (453)
Samples

Figure 7.